SAFE WAVE

STREAMLIING THE ASSESSMENT OF ENVIRONMENTAL EFFECTS OF WAVE ENERGY

DELIVERABLE 3.1
EMF Modelling

This Project is co-funded by the European Climate, Infrastructure and Environment Executive Agency (CINEA)

WP 3
Deliverable 3.1 EMF Modelling

Lead partner for deliverable:
WavEC

AUTHORS
Alessandra Imperadore, WavEC
Luis Amaral, WavEC
Pedro Almeida Vinagre, WavEC

SUBMISSION DATE
28 | November | 2024

DISSEMINATION LEVEL

PU	Public	X
CL	Classified – EU classified (EU-CONF, EU-RESTR, EU-SEC) under Commission Decision No 2015/444	
CO	Confidential, only for members of the consortium (including Commission Services)	

DOCUMENT HISTORY

Issue Date	Version	Changes Made / Reason for this Issue
04/04/2023	1.00	First version
28/11/2024	2.00	Final Version

CITATION

Imperadore, A., Amaral, L., Vinagre, P.A., 2024. Deliverable 3.1 EMF Modelling. Corporate deliverable of the SafeWAVE Project co-funded by the European Climate, Infrastructure and Environment Executive Agency (CINEA), Call for Proposals EMFF-2019-1.2.1.1 - Environmental monitoring of ocean energy devices. 50 pp. DOI: http://dx.doi.org/10.13140/RG.2.2.17733.77281

This Project is co-funded by the European Climate, Infrastructure and Environment Executive Agency (CINEA), Call for Proposals EMFF-2019-1.2.1.1 - Environmental monitoring of ocean energy devices.

CONTENTS

1. SafeWAVE project synopsis 4
2. Glossary 7
3. Executive summary 8
4. Submarine Power Cables 9
4.1 CPO Submarine Power Cable 11
4.2 BiMEP Submarine Power Cable 11
4.3 SEM-REV Submarine Power Cable 13
4.3.1 SEM-REV Submarine Dynamic Power Cable 14
4.3.2 SEM-REV Submarine Export Power Cable 14
5. EMF Modelling 17
5.1 Theory 17
5.1.1 Magnetic fields 18
5.1.2 Electric fields 19
5.2 FEMM Model 21
5.3 Case studies 21
5.3.1 Aguçadoura 23
5.3.2 BiMEP 27
5.3.3 SEM-REV Dynamic cable 30
5.3.4 SEM-REV Export cable 35
6. Validation 39
6.1 SEM-REV cable model validation 39
7. Discussion and Conclusions 43
8. References 46
9. Annex I 49

1. SafeWAVE project synopsis

The European Atlantic Ocean offers a high potential for marine renewable energy (MRE), which is targeted to be at least 32% of the EU's gross final consumption by 2030 (European Commission, 2020). The European Commission is supporting the development of the ocean energy sector through an array of activities and policies: the Green Deal, the Energy Union, the Strategic Energy Technology Plan (SET-Plan) and the Sustainable Blue Economy Strategy. As part of the Green Deal, the Commission adopted the EU Offshore Renewable Energy Strategy (European Commission, 2020) which estimates to have an installed capacity of at least 60 GW of offshore wind and at least 1 GW of ocean energy by 2030, reaching 300 GW and 40 GW of installed capacity, respectively, moving the EU towards climate neutrality by 2050.

Another important policy initiative is the REPowerEU plan (European Commission, 2022) which the European Commission launched in response to Russia's invasion of Ukraine. REPowerEU plan aims to reduce the European dependence amongst Member States on Russian energy sources, substituting fossil fuels by accelerating Europe's clean energy transition to a more resilient energy system and a true Energy Union. In this context, higher renewable energy targets and additional investment, as well as introducing mechanisms to shorten and simplify the consenting processes (i.e., 'go-to' areas or suitable areas designated by a Member State for renewable energy production) will enable the EU to fully meet the REPowerEU objectives.

The nascent status of the Marine Renewable Energy (MRE) sector and Wave Energy (WE) in particular, yields many unknowns about its potential environmental pressures and impacts, some of them still far from being completely understood. Wave Energy Converters' (WECs) operation in the marine environment is still perceived by regulators and stakeholders as a risky activity, particularly for some groups of species and habitats.

The complexity of MRE licensing processes is also indicated as one of the main barriers to the sector development. The lack of clarity of procedures (arising from the lack of specific laws for this type of projects), the varied number of

authorities to be consulted and the early stage of Marine Spatial Planning (MSP) implementation are examples of the issues identified to delay projects' permitting.

Finally, there is also a need to provide more information on the sector not only to regulators, developers and other stakeholders but also to the general public. Information should be provided focusing on the ocean energy sector technical aspects, effects on the marine environment, role on local and regional socio-economic aspects and effects in a global scale as a sector producing clean energy and thus having a role in contributing to decarbonise human activities. Only with an informed society would be possible to carry out fruitful public debates on MRE implementation at the local level.

These non-technological barriers that could hinder the future development of WE in EU, were addressed by the WESE project funded by European Maritime and Fisheries Fund (EMFF) in 2018. The present project builds on the results of the WESE project and aims to move forward through the following specific objectives:

1. Development of an **Environmental Research Demonstration Strategy** based on the collection, processing, modelling, analysis and sharing of environmental data collected in WE sites from different European countries where WECs are currently operating (Mutriku power plant and BiMEP in Spain, Aguçadoura in Portugal and SEMREV in France); the SafeWAVE project aims to enhance the understanding of the negative, positive and negligible effects of WE projects. The SafeWAVE project will continue previous work, carried out under the WESE project, to increase the knowledge on priority research areas, enlarging the analysis to other types of sites, technologies and countries. This will increase information robustness to better inform decision-makers and managers on real environmental risks, broad the engagement with relevant stakeholders, related sectors and the public at large and reduce environmental uncertainties in consenting of WE deployments across Europe;
2. Development of a **Consenting and Planning Strategy** through providing

guidance to ocean energy developers and to public authorities tasked with consenting and licensing of WE projects in France and Ireland; this strategy will build on country-specific licensing guidance and on the application of the MSP decision support tools (i.e. WEC-ERA[1] by Galparsoro et al., 2021[2] and VAPEM[3] tools) developed for Spain and Portugal in the framework of the WESE project; the results will complete guidance to ocean energy developers and public authorities for most of the EU countries in the Atlantic Arch.

3. Development of a **Public Education and Engagement Strategy** to work collaboratively with coastal communities in France, Ireland, Portugal and Spain, to co-develop and demonstrate a framework for education and public engagement (EPE) of MRE enhancing ocean literacy and improving the quality of public debates.

[1] https://aztidata.es/wec-era/;
[2] Galparsoro, I., M. Korta, I. Subirana, Á. Borja, I. Menchaca, O. Solaun, I. Muxika, G. Iglesias, J. Bald, 2021. A new framework and tool for ecological risk assessment of wave energy converters projects. Renewable and Sustainable Energy Reviews, 151: 111539
[3] https://aztidata.es/vapem/

2. Glossary

µT	Microtesla(s)
A	Ampere
BiMEP	Biscay Marine Energy Platform
CPO	CorPower Ocean
EMF	Electromagnetic field(s)
Hz	Hertz
HVAC	High Voltage Alternate Current
h	hour(s)
kg	Kilogram(s)
kV	Kilovolt(s)
kW	Kilowatt(s)
m	Metre(s)
mm	Millimetre(s)
MRE	Marine Renewable Energy
nT	Nanotesla(s)
SafeWAVE	Streamlining the Assessment of Environmental Effects of Wave Energy
ROV	Remotely Operated Vehicle
WE	Wave Energy
WESE	Wave Energy in Southern Europe
μ	Magnetic Permeability
$\mu V/m$	MicroVolt(s)/meter
σ	Electrical Conductivity

3. Executive summary

The SafeWAVE project aims to improve the knowledge on the potential environmental impacts from Wave Energy (WE) projects. In the project scope, Work Package 3 aims to model environmental data related to: i) Electromagnetic Fields, ii) Sound propagation and iii) Marine dynamics.

This deliverable reports the works of Task 3.1 related to the modelling of the electromagnetic fields emitted by subsea power cables. The main goal of Task 3.1 is to estimate the magnetic and electric fields amplitude generated by the power cables at the three test sites under study: Aguçadoura, BiMEP and SEM-REV. This was achieved using the open-source tool developed within the WESE project which consists of an EMF modelling tool based on Python code and FEMM software. Despite the tool could not be validated when created, the code was adapted for the purpose of this task, and it was validated using the data collected during the monitoring campaign performed within WP2 (Task 2.2).

4. Submarine Power Cables

Spanning over dozens of kilometres, subsea (or submarine) power cables are undoubtably the main source of EMF generated by offshore energy projects. This section presents the main characteristics of submarine power cables which are relevant for understanding the EMF modelling work presented in this report.

Subsea power cables are composed of several layers. The overall design and materials do not differ much from cables installed ashore. Figure 1 illustrates the main components of a conventional three-phase HVAC submarine power cable. Although the conductors can be made of alternatives like aluminium, the most frequently applied material is copper. These can either be composed of one single wire, stranded conductors, or profiled wire conductors, which provide a very smooth conductor surface.

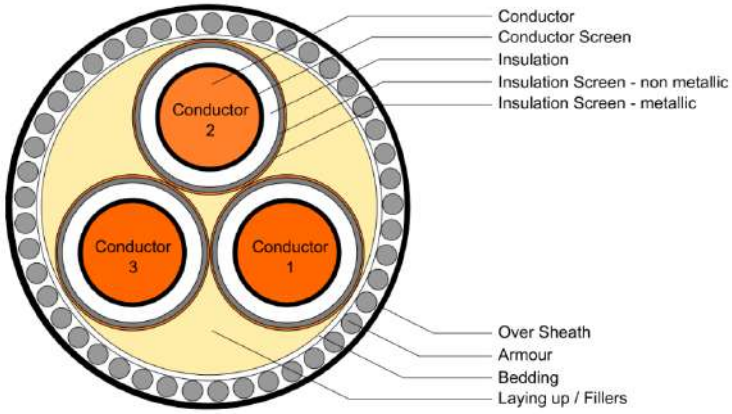

Figure 1. Typical 3-Phase Submarine Power Cable Sketch [IEC 605202-2].

Due to the applied electric potential, the conductors must be insulated by a proper dielectric material, with cross-linked polyethylene (XLPE) being a common material used for the insulation. Besides its favourable dielectric properties, it is characterized by a comparatively high resistance to heat (operating temperature around 90°). Additionally, the insulation is coated with two 1-2 mm thick layers (insulation and conductor screen). They guarantee a smooth surface, which results in decreased local stress enhancements, like notch effects. The screens thus improve the insulation durability by maintaining both mechanical properties and the related dielectric strength.

The laying up consists of fillers, which define the cylindrical cable shape and add flexibility. It is enclosed by the bedding, which serves as an underlaying sheet for the armouring. The latter comprises a bundle of round wires with a diameter of two up to eight millimetres. The armour provides tension stability and mechanical protection during installation and operation (e.g. against fishing gear or anchors). It is the only element with physical properties and dimensions that affect significantly the internal and surrounding magnetic field. This property is referred to as magnetic permeability (μ), which defines the ability of a material to support the formation of a magnetic field within itself, thus, the higher the value the less resistant is the material to the passage of magnetic field lines. Table 1 shows the magnetic permeability and conductivity values of typical materials used in the construction of subsea cables. However, these should be accounted as average values only, since this property is typically nonlinear in ferromagnetic materials, and varies significantly with the magnetic field strength.

Table 1. Electromagnetic properties for cable components (CMACS, 2003).

	Magnetic Permeability μ	**Conductivity σ**
Conductor (copper)	1.0	58.000.000
XLPE	1.0	0.0
Sheath (polyethylene)	1.0	0.0
Armour (steel)	300	110.000
Seawater	1.0	5.0
Seabed	1.0	1.0

The armour can be made of ferrous (such as electric steel) or non-ferrous (such as copper) materials. Due to its relatively high magnetic permeability, ferrous materials concentrate the magnetic field around them, which reduces the magnetic field outside of the power cable. It is to be noted that the armour is the only magnetic material in the cable that can, therefore, contain the magnetic field within it.

4.1 CPO Submarine Power Cable

The power cable at the Aguçadoura test site under study is the export cable connecting the HiWave-5 device to the onshore substation.

The export cable is laid on the seabed and it is a three-phase, medium voltage with a double armouring layer and an optical fibre unit.

For confidentiality reasons the sketch of the cable cannot be shared, therefore the one in Figure 2 is a generic drawing.

Table 2 reports the electrical specifications and the geometry dimensions needed as inputs for the modelling tool.

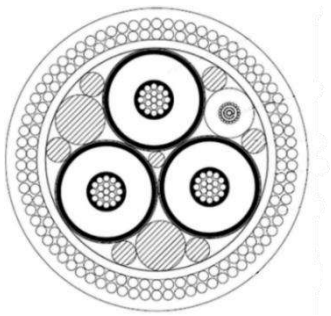

Figure 2. Generic sketch of a three-phase, double-armour power cable. (Source: CPO)

4.2 BiMEP Submarine Power Cable

The BiMEP test site have 4 similar submarine power cables installed. These can be described as double armour, medium voltage power cables with an optical fibre unit, and 2 low voltage auxiliary power cables (Figure 3). Relevant cable characteristics for the EMF studies are (Table 3): the overall cable dimensions, the armouring material and thickness, the conductor's distance (due to the cancelling effect of the current lag between the three-phases), and any ferromagnetic metallic screens. This cable, as shown in Figure 3, has an overall diameter of 108 mm, is composed of a double armour of approximately 60 and 69 galvanized steel wires, a three-phase 8.7/15 kV export capacity composed of 3 stranded copper conductors with 185 mm^2 cross section and XLPE insulation. For modelling simplicity, the 0.6/1 kV auxiliary power cable will not be considered in this study.

Table 2. CPO export cable specifications. (Source: CPO).

Submarine Power Cable General Specifications		
Rated Voltage	3.6/6(7.2) kV	
Cable ampacity (seabed soil 25 °C)	274 A	
Overall diameter	92.5 mm	
Subsea Cable Components	**Material**	**Dimension**
Conductor	Copper	Φ 11.6 mm
Conductor screen	Semi-conducting compound	0.7 mm
Conductor insulation	XLPE	2.7 mm
Conductor insulation non-metallic screen	Semi-conducting compound	0.7 mm
Conductor insulation metallic screen	Copper	Φ 0.8 mm
Conductor outer sheath	Polyethylene	1.7 mm
Bedding	HDPE	3.0 mm
Armour 1st layer	Galvanized steel wires	Φ 3.15 mm
Armour 2nd layer	Galvanized steel wires	Φ 3.15 mm
Over sheath	HDPE	5.0 mm
Burial depth	-	-

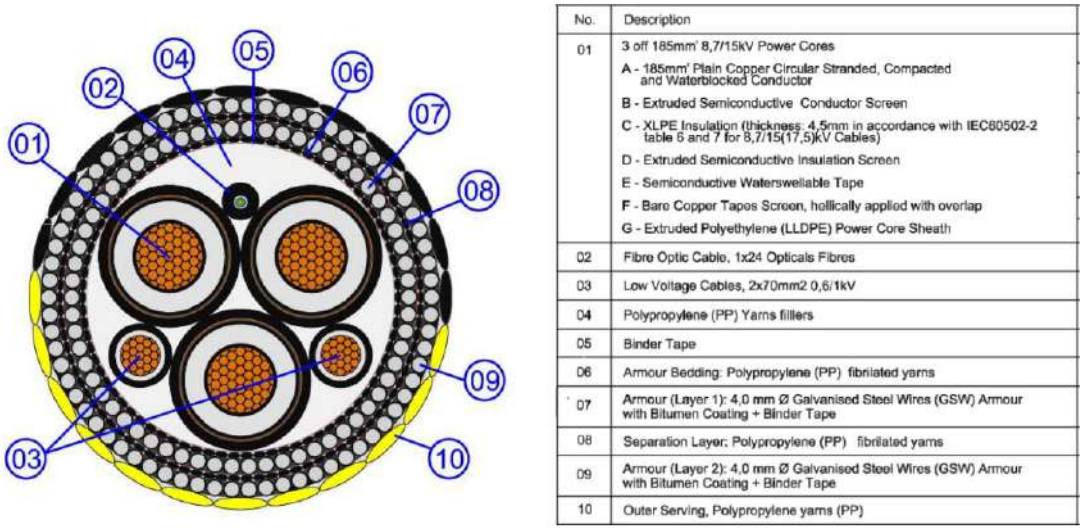

No.	Description
01	3 off 185mm² 8,7/15kV Power Cores A - 185mm² Plain Copper Circular Stranded, Compacted and Waterblocked Conductor B - Extruded Semiconductive Conductor Screen C - XLPE Insulation (thickness: 4,5mm in accordance with IEC60502-2 table 6 and 7 for 8,7/15(17,5)kV Cables) D - Extruded Semiconductive Insulation Screen E - Semiconductive Waterswellable Tape F - Bare Copper Tapes Screen, hollically applied with overlap G - Extruded Polyethylene (LLDPE) Power Core Sheath
02	Fibre Optic Cable, 1x24 Opticals Fibres
03	Low Voltage Cables, 2x70mm2 0,6/1kV
04	Polypropylene (PP) Yarns fillers
05	Binder Tape
06	Armour Bedding: Polypropylene (PP) fibrilated yarns
07	Armour (Layer 1): 4,0 mm Ø Galvanised Steel Wires (GSW) Armour with Bitumen Coating + Binder Tape
08	Separation Layer: Polypropylene (PP) fibrilated yarns
09	Armour (Layer 2): 4,0 mm Ø Galvanised Steel Wires (GSW) Armour with Bitumen Coating + Binder Tape
10	Outer Serving, Polypropylene yarns (PP)

Figure 3. BiMEP submarine power cable sketch. (Source: Chainho and Bald, 2021).

Table 3. BiMEP cable specifications and components. (Source: Chainho and Bald, 2021).

Submarine Power Cable General Specifications		
Rated Voltage	8.7/15 (17.5) kV	
Current carrying capacity	422 A	
Overall diameter	108 mm	
Overall weight (air)	25.5 kg/m	
Overall weight (water)	18.5 kg/m	
Subsea Cable Components	**Material**	**Dimension**
Conductor	Plain copper wires	Φ 15.9 mm
Conductor screen	Extruded semi-conducting compound	1.0 mm
Insulation	XLPE compound	4.5 mm
Insulation Screen	Extruded semi-conducting compound	1.0 mm
Metallic Screen	1 layer with 2 bare copper tapes	0.1 mm
Inner Sheath	Polyethylene LLDPE	2.2 mm
Bedding	Polypropylene strings	2.0 mm
Wire Armour Layer 1	Galvanized steel wires	Φ 4.0 mm
Separation Layer	Polypropylene strings	2.0 mm
Wire Armour Layer 2	Galvanized steel wires	Φ 4.0 mm
Outer Sheath	Polypropylene strings	3.0 mm
Burial depth	-	-

4.3 SEM-REV Submarine Power Cable

At SEM-REV test site the specifications from two power cables are available and were therefore modelled.

- Submarine dynamic power cable: it is the 5 MVA, three-phase, double armour umbilical cable that connects the energy device to the collection hub.
- Submarine export power cable: it is the 8 MVA three-phase, single armour export cable that connects the collection hub to the onshore substation.

4.3.1 SEM-REV Submarine Dynamic Power Cable

The submarine power cable installed in SEM-REV test site is a dynamic cable connecting the energy device to a collection hub, which is connected with a static export cable to shore. The cable is a three-phase, double-armour, medium voltage with an optical fibre unit (Figure 4).

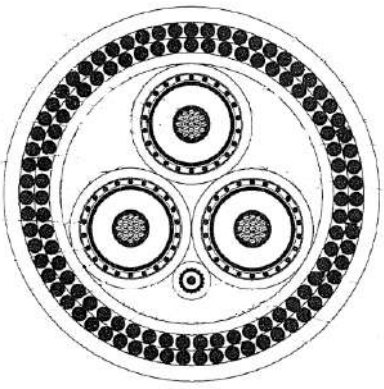

Figure 4. SEM-REV submarine dynamic power cable sketch. (Source: ECN).

Despite the cable being laid on the seabed, natural burial was observed during the last ROV inspection. Since it was not possible to quantify the burial, in the modelling the cable is assumed to be surrounded by seawater. Moreover, in the space between the armouring layer it is plausible to assume some seawater infiltration since that section of the cable is not waterproof.

Table 4 presents the specifications needed for the purpose of the modelling.

4.3.2 SEM-REV Submarine Export Power Cable

The cable is a three-phase, single-armour, medium voltage with an optical fibre unit (Figure 5, Table 5). This cable connects the hub to the onshore substation.

The export cable is buried for most of its length (23km), except for two sections (72m long and 288m long) where concrete mattresses reinforce the protection of the cable. The burial depth ranges from 1m to 1.5m. In Table 5, the specifications needed for the modelling are presented.

Table 4. SEM-REV test site dynamic cable specifications. (Source: ECN).

Submarine Power Cable General Specifications		
Rated Voltage	12/20 (24) kV	
Current ampacity (seabed soil 25 °C)	246 A	
Overall diameter	102 mm	
Subsea Cable Components	**Material**	**Dimension**
Conductor cross sectional area	Copper	50 mm^2
Conductor screen	Polyethylene	1.0 mm
Conductor insulation	XLPE	5.5 mm
Conductor insulation non-metallic screen	Semi-conducting screen	1.0 mm
Conductor insulation metallic screen	Copper	Φ 1.44 mm
Conductor outer	HDPE	2.0 mm
Bedding thickness	HDPE	3.0 mm
Armour 1st layer thickness	Galvanized steel wires	Φ 4.0 mm
Armour 2nd layer thickness	Galvanized steel wires	Φ 4.0 mm
Over sheath thickness	HDPE	4.3 mm
Burial depth	-	-

Figure 5. SEM-REV submarine export power cable sketch. (Source: ECN).

Table 5. SEM-REV test site export cable specifications. (Source: ECN).

Submarine Power Cable General Specifications		
Rated Voltage	12/20 (24) kV	
Overall diameter	86 mm	
Subsea Cable Components	**Material**	**Dimension**
Conductor cross sectional area	Class 2 water blocked copper	Φ 11.6 (19 strands)
Conductor screen	Extruded semi conductive compound	1.0 (assumed)
Conductor insulation	XLPE	5.5 mm
Conductor insulation non-metallic screen	Extruded semi conductive compound	1.0 (assumed)
Conductor insulation metallic screen	Individual screen on each phase.	0.1mm
Conductor outer	PE	2.0mm
Bedding thickness	PE	1.8 mm
Armour 1st layer thickness	Galvanized steel wires	Φ 4.5
Armour 2nd layer thickness	-	**-**
Over sheath thickness	PE	3.2 mm
Burial depth	-	1-1.5 m

5. EMF Modelling

5.1 Theory

Energized subsea power cables are known sources of EMF. As introduced in Deliverable 2.1 (Vinagre et al., 2021), the EMF can be described as a physically significant field generated by an electric charge. As the name suggests, EMF can be viewed as combination of two individual fields: the electric field ($\vec{\boldsymbol{E}}$) and the magnetic field ($\vec{\boldsymbol{B}}$), which are mutually dependent. The magnetic fields can be generated by electric charges in motion (electric current) by varying electric fields and by the intrinsic magnetic moments of a magnetic material (e.g. permanent magnets). Electric fields are of two kinds: Electrostatic field -> produced by stationary electric charges (e.g. electric potential difference – or voltage) and induced electric field -> produced by time-varying magnetic fields. All these phenomena are present in energized subsea power cables.

Electrostatic fields are confined between conductive elements with an electric potential difference. Since subsea cable conductors have a metallic shield covering the insulation which is generally grounded (zero potential), this guarantees the electric field is confined within the insulation. On the other hand, energized cables produce a magnetic field proportional to cable current. These magnetic field lines will be concentrated around materials with high magnetic permeability, thus, any ferromagnetic materials present in the cable, such as some types of cable armouring, will have an attenuation effect concerning the field intensity outside of the cable. Despite this attenuation effect, magnetic field lines are not fully contained within the cable.

Since the subsea power cables in this study have AC profiles, a time-varying magnetic field is expected outside of the cable, which induces electric fields as predicted by Maxwell equations. The Maxwell equations, considered among the most important scientific equations, set the base for understanding the EMF theory. The following sections present a summary of the most relevant aspects to consider when attempting to model EMF, for the particular case of submarine power cables.

5.1.1 Magnetic fields

The baseline to quantify the magnetic field intensity outside of a power cable is described by the Ampere-Maxwell law. This law states "A circulating magnetic field is produced by an electric current and by an electric field that changes with time" (Fleisch, 2008). The corresponding equation quantifies the magnetic field by the sum of two terms, one proportional to the electric current, and another to the rate of change of an electric field. Minding that magnetic fields induced by changing electric fields are extremely weak (mostly relevant to problems at radio frequency levels, i.e. from kHz to GHz), the latter term can be neglected for the specific case of subsea power cables (Meeker, 2019) which operate at 50 Hz or 60 Hz. Thus, for our problem the formula can be simplified, leaving only the terms associated with the Ampere law equation:

$$\oint_C \vec{B} \cdot \vec{dl} = \mu I_{enc} \qquad \text{(Eq. 1)}$$

where, $\oint_C$ is the line integral around the closed curve C, $\vec{B}$ is the resultant vector of the magnetic field at the point of calculation (in Tesla units), $\vec{dl}$ is an infinitesimal element of the curve C (in metres), μ is the magnetic permeability of the medium (where in vacuum $\mu = \mu_r \mu_0 = 1x4x10^{-7}\mathrm{H/m}$) and I_{enc} the current flowing through the closed curve C (in Ampere units). For better understanding how this formula applies to a subsea power cable, an infinite long and straight conductor will be assumed. When this conductor carries a current I, the resulting magnetic field lines are concentric circles surrounding the conductor centre, as shown in Figure 6.

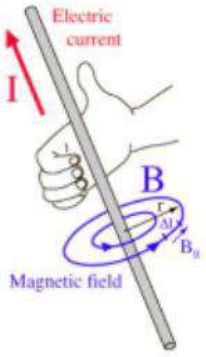

Figure 6. Magnetic field lines surrounding a straight long conductor, as per the *Right hand rule* mnemonic.

The amplitude of $\vec{B}$ is the same in every point of the concentric circle with radial distance r, meaning the line integral from Amper law is equal to the sum of the magnetic field vector along the concentric circle, which returns $\oint_C \vec{B} \cdot \vec{dl} = B(2\pi r)$. The magnetic field for this problem can then be computed with the following:

$$\vec{B} = \frac{\mu I}{2\pi r}\hat{\phi} \qquad \text{(Eq. 2)}$$

with the direction being unit vectors $\hat{\phi}$ tangential to the concentric circle, shown in Figure 6 as per the right-hand rule. The problem described in the previous paragraphs assumes a single long and straight conductor; however, as presented in section 4, submarine power cables are usually part of a three-phase power system, with the three conductors placed symmetrically inside the subsea cable. In this case, these three conductors carry a three-phase current which individually generate magnetic field lines with the same properties as described in (Eq. 2). These fields are added together to the resulting magnetic field, which is the sum of the individual vector fields generated from the cable conductors. As described by (Eq. 2), the contribution of each individual conductor to the magnetic field is dependent on the distance of each conductor to the point of measurement, and the amplitude of the current at the time of measurement. Assuming an arbitrary point of measurement P, the magnetic field as per (Eq. 2), can be computed from the instant current amplitude at each of the 3 conductors, and the distance from the conductors. Mathematically this complex interaction can be described as a superposition of three single fields surrounding their respective conductors. Figure 7 provides a visual representation.

5.1.2 Electric fields

There are two different sources of electric fields, one created by stationary electric charges, referred to as electrostatic field and one created by a changing magnetic field, referred to as induced electric field. Both are vector units with a direction and magnitude, measured in $\mathrm{V/m}$, with the net value at any point being the vector sum of all the electric fields present at that point. An electrostatic field is present in all live power cables, as the system voltage

results in an electric potential difference between the conductors and the remaining environment. Nowadays, it is a common practice to ground the conductor metallic sheathes (for safety and reliability purposes) which guarantees this component has a zero-electric potential. This confines the electrostatic field within the individual conductors, as this E-field will be radially distributed inside the dielectric insulation from the conductor core to the metallic sheathes. Therefore, this E-field source is not expected outside of the cable if proper cable earthing is achieved (CMASC, 2003). Thus, for AC subsea power cables, only electric field produced by the varying magnetic field is emitted into the marine environment. The Faraday law of induction sets the base to understand this principle.

$$\oint_C \vec{E} \cdot \overrightarrow{dl} = -\frac{d}{dt} \int_S \vec{B} \cdot \hat{n}\, da \qquad \text{(Eq. 3)}$$

This law states "A circulating electric field is produced by a magnetic field that changes with time" (Fleisch,2008). Also relevant to our case, is to mention that an electric field applied to a conductive medium (e.g. seawater) will cause electric currents to flow in that material, hence, the electric current density is directly proportional do the electrical field: $J=\sigma\vec{E}$, with the constant of proportionality being the medium conductivity.

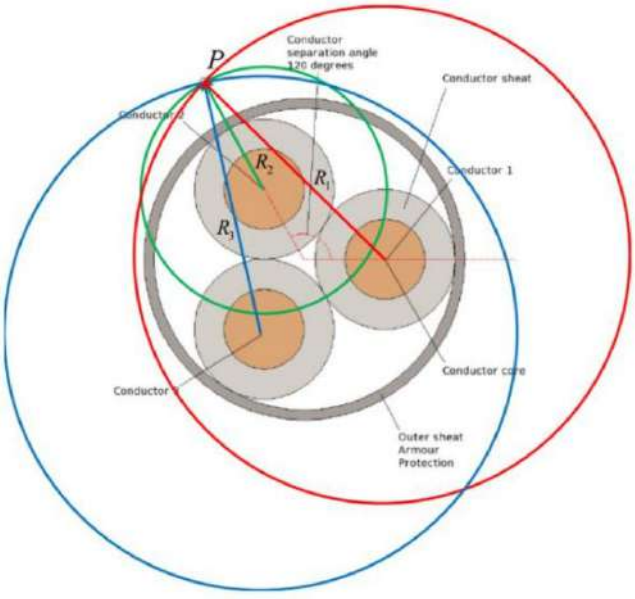

Figure 7. Three-phase cable cross-section, with P being the point of measurement, and R1, R2, and R3 the distance from the conductors to the point of measurement.

5.2 FEMM Model

The differential equations shown in the previous section appear to be relatively compact; however, the complexity of combining a three-phase system and cable geometries with different materials (e.g. steel and copper) within different mediums (e.g. seabed and seawater), suggested that a finite element method should be used to model this problem.

The open-source tool developed within the WESE project was used and adapted to suit the case studies considered in the SafeWAVE project. The tool is presented in Chainho and Bald (2021) and is based on Python and FEMM, which is a simple and low computation cost software package for solving electromagnetic projects using the finite element method. Figure 8 presents the flowchart of the tool structure. As expected, the algorithm follows closely FEMM's processing routines, adapted specifically for the design and analysis of subsea power cables.

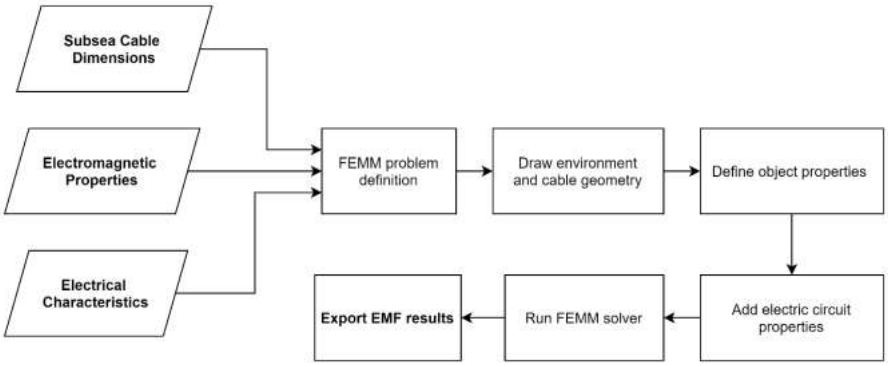

Figure 8. EMF modelling tool flowchart.

5.3 Case studies

The SafeWAVE project scope includes three submarine power cables at three different test sites, namely: the export cable in the Aguçadoura test site in Portugal, one of the cables in the BiMEP test site in Spain, and the dynamic cable in the SEM-REV test site in France. As explained in D2.2 (Imperadore et al., 2023) during the monitoring campaign at the SEM-REV test site the export cable was also depicted and therefore its modelling is included in this present deliverable.

As defined in D2.2 (Imperadore et al., 2023), in-situ underwater EMF monitoring campaigns were foreseen at each of the three test sites to acquire data for validating the model. Additionally, EMF monitoring was planned in Aguçadoura onshore at the substation. The aim was to acquire EMF data during low and high sea states, allowing to improve the tool and assess the feasibility of using onshore data instead of offshore underwater data for future monitoring of EMF.

However, the data validation could not be done for either the BiMEP or Aguçadoura test sites. Regarding BiMEP, EMF data could not be collected for the following reasons: (1) within the WESE project the survey was carried out during a calm sea state producing data not relevant for validating the model, and (2) within the SafeWAVE project the data could not be collected because at the time of the campaign the device had already been decommissioned. In the case of Aguçadoura, CPO's device C4 was removed from the site due to maintenance purposes and was not redeployed within the SafeWAVE project timeline.

Therefore, only the SEM-REV cables (dynamic and export) modelling was validated. For each case study three different conditions were simulated corresponding to different currents in A:

1- Simulation using the levels acquired during the monitoring survey for the model validation, when possible. The results from the model validation are found in section 6 .

2- Simulation using the current carrying capacity or ampacity indicated in the cable specifications. The results of this simulation are of great relevance in the perspective of upscaling to MRE farms which will lead to the full exploitation of the cable capacity. The results can be found in the present section.

3- Simulation per current unit. As seen in section 5.1 the magnetic field is linearly proportional to the current, therefore these results can be used as a base value to estimate the EMF amplitude at any current value. The results can be found in this present section.

Each simulation provides information about the magnitude of the magnetic and electric field at different distances from the cable surface. The decay of the EMF is proportional to the square of the distance; once again, in perspective of larger MRE farms, this data can help understanding at which distance to install potential new power cables in order to avoid the overlaid of fields.

5.3.1 Aguçadoura

The power cable under study is the export cable connecting the HiWave-5 wave energy device to the substation onshore. The cable is laid on the surface but since it was installed in January 2022 some natural burial shall be assumed. Despite this, the natural burial cannot be quantified therefore it is not modelled in the tool, but some water infiltration within the armouring layers is considered.

The model was created using the open-source tool described in section FEMM Model; based on the cable geometry (

Table 2) a phase current is applied and the FEMM solver computes the EMF radiated as shown in the Figure 9.

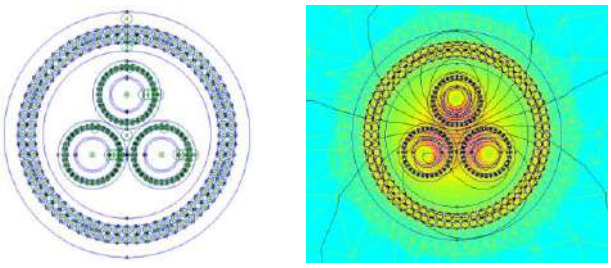

Figure 9. CPO cable model in FEMM (left), Finite Element Analysis in FEMM (right).

Below, the results from two simulations are reported, namely:

- Electric and magnetic field at maximum continuous current (Figure 10)
- Electric and magnetic field per current unit (Figure 11).

Figure 10 presents the most relevant results which allow estimating the maximum EMF values to be expected when the cable is used at its maximum continuous current. From

Table 2, the cable ampacity is known and equal to 274 A.

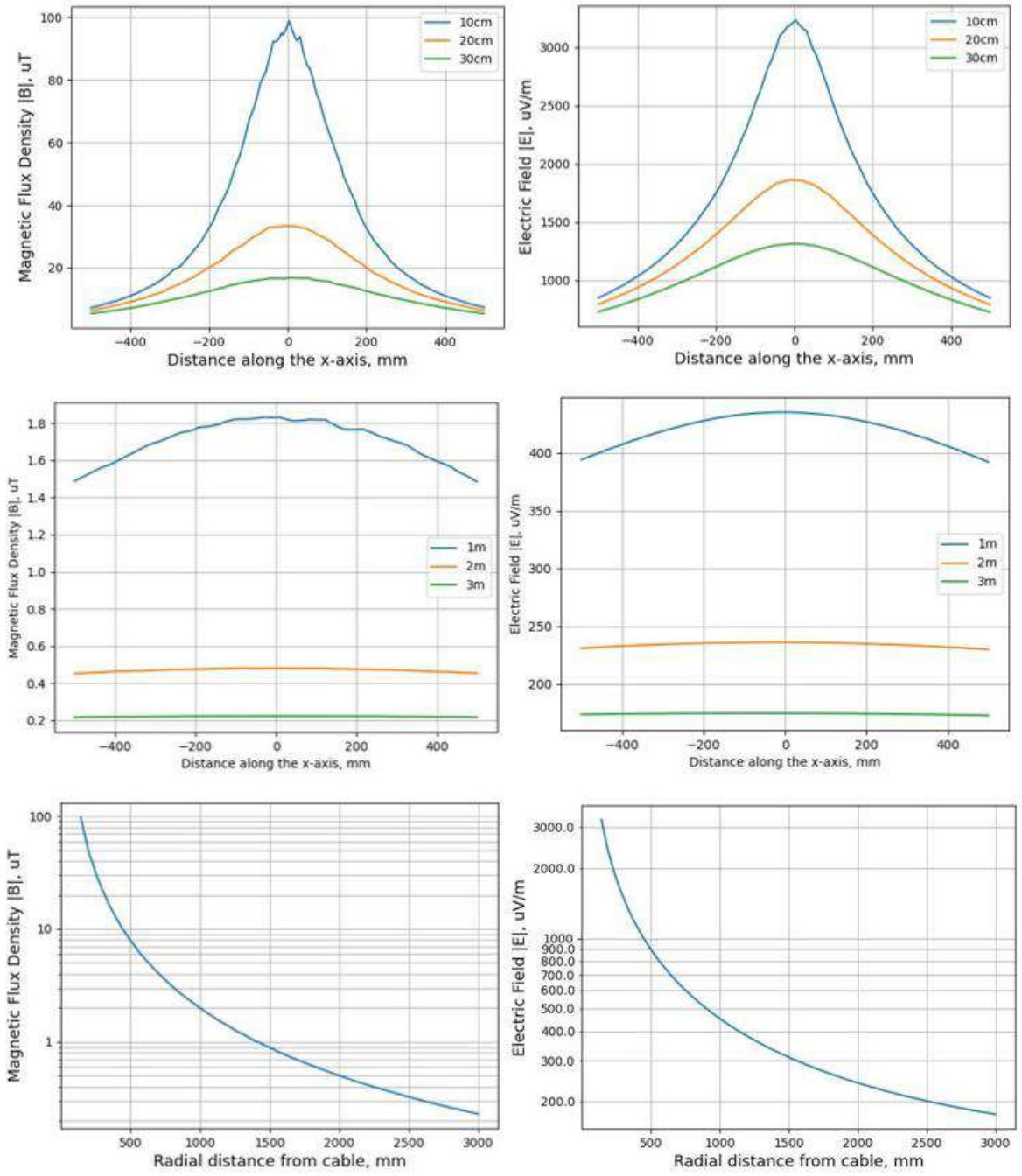

Figure 10. EMF modelling results from CPO submarine power cable at cable ampacity at 10, 20, and 30 cm parallel to the cable surface (top); at 1, 2, and 3 m parallel to the cable surface (middle); and at a radial distance from the cable surface (bottom).

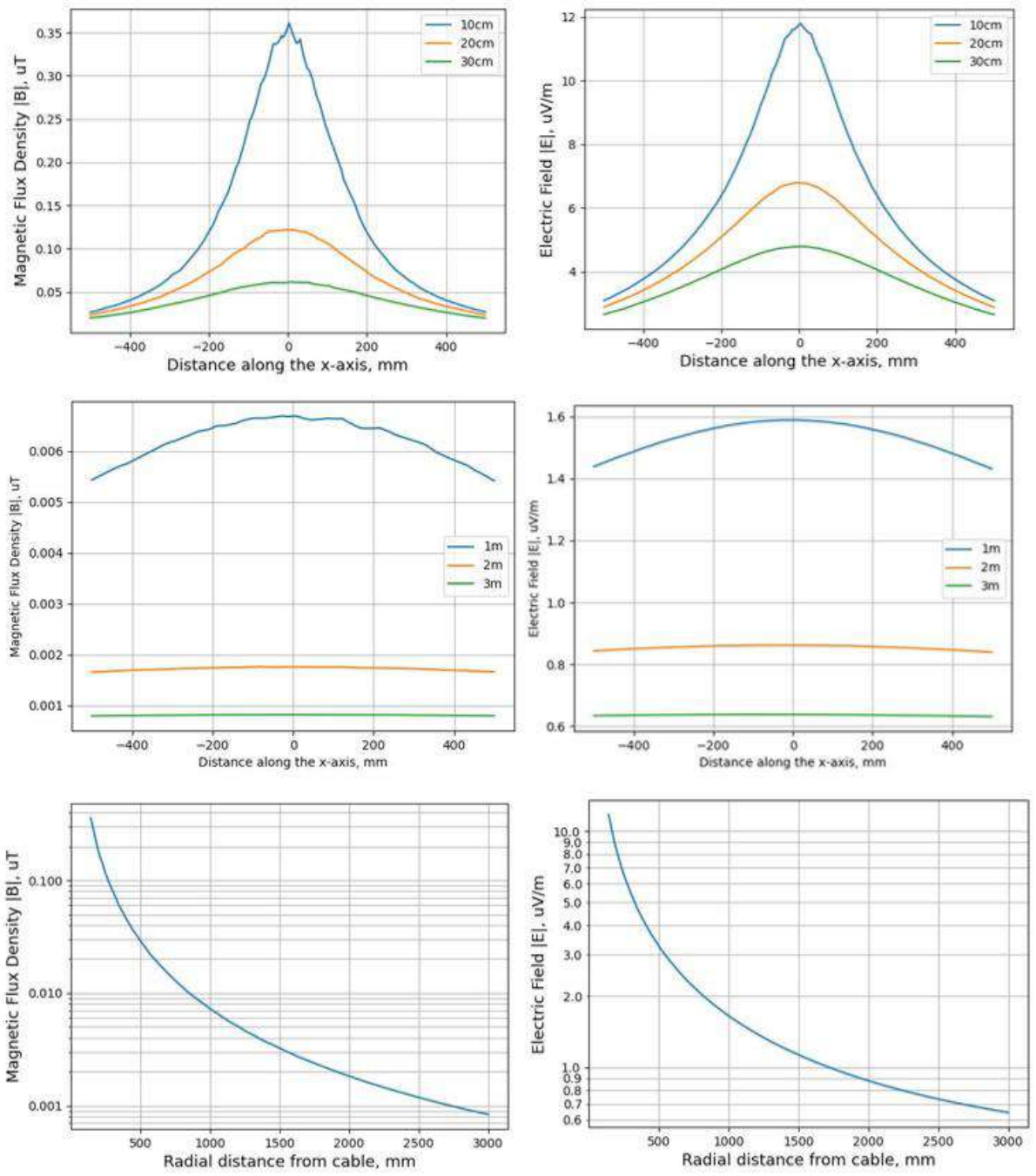

Figure 11. EMF modelling results from CPO submarine power cable per current unit at a distance of 10, 20, and 30 cm parallel to the cable surface (top); at a distance of 1, 2, and 3 m parallel to the cable surface (middle); and at a radial distance from the cable surface (bottom).

At 10 cm from the cable, the flux density $|B|$ reaches 98.85 μT, and at a 3 m distance it reduces to 0.22 μT. The electric field follows the same trend, it reaches its maximum value of 3232.10 $\mu V/m$ at 10 cm from the cable and decays to 174.84 $\mu V/m$ at 3 m distance.

Figure 11 shows results per current unit which can be used to estimate the magnitude of EMF at any current level. Within the project scope, it is relevant to estimate the EMF emissions when the device under study is at its rated power.

As depicted in D2.1 (Vinagre et al., 2021), at the Aguçadoura test site the device under study is the HiWave-5, a wave energy device whose electrical specifications are reported in Table 6. HiWave-5 electrical specifications.

Table 6. HiWave-5 electrical specifications

	P **Device Rated Power**	**VLL** **Transmission Voltage**	**I** **Phase Current**
HiWave-5	300 kW	6 kV	28.9 A

Considering the following equation for a three-phase system $P = \sqrt{3} \cdot V_{LL} \cdot I \cdot pf$, where P is the power capacity, V_{LL} is the line-to-line voltage, I is the phase current and pf is the power factor assumed equal to one, the phase current is obtained. All results for the three conditions considered (cable rated current, unit current and device rated current) are summarized in Table 7.

Table 7. Summary of the results at the Aguçadoura test site.

	Phase current	**|B| at 10 cm**	**|B| at 3 m**	**|E| at 10 cm**	**|E| at 3 m**
Cable ampacity	274 A	98.85 μT	0.22 μT	3232.10 $\mu V/m$	174.84 $\mu V/m$
Unit current	1 A	0.36 μT	0.0008 μT	11.80 $\mu V/m$	0.63 $\mu V/m$
Device max. current	28.9 A	10.43 μT	0.02 μT	340.90 $\mu V/m$	18.44 $\mu V/m$

Annex I, results at 20 cm, 30 cm, 1 m, and 2 m are also provided

5.3.2 BiMEP

As mentioned in section 4.2, at the test site there are four equal subsea cables and the specifications were taken from the WESE deliverable D3.1 (Chainho and Bald, 2021) (Table 3). Figure 12 shows the sketch of the cable under study, the cable model and its Finite Element Analysis using FEMM software.

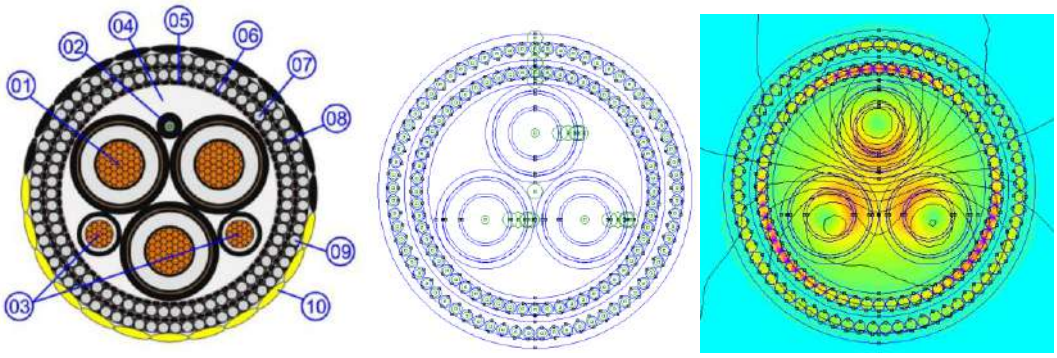

Figure 12. BiMEP cable model sketch (left), cable model on FEMM (middle), Finite Element Analysis in FEMM (right).

Below, the results from two simulations are reported, namely:

- Electric and magnetic field at current carrying capacity (Figure 13).
- Electric and magnetic field per current unit (Figure 14).

Figure 13 presents the most relevant results as it allows to estimate the maximum EMF values to be expected when the cable is used at its current carrying capacity. From Table 3 the current carrying capacity is known and equal to 422 A.

At 10 cm from the cable the flux density |B| reaches 152.37 μT and at 3 m it reduces to 0.40 μT. The electric field follows the same trend, reaching maximum 5500.57 μV/m and decaying to 334.33 μV/m at 3 m (Table 8).

Figure 14 shows results per current unit. As depicted in D2.1 (Vinagre et al., 2021), at the BiMEP test site the device under study was the Penguin II, a wave energy device with the electrical specifications reported in Table 9.

Considering the following equation $P = \sqrt{3} \cdot V_{LL} \cdot I \cdot pf$ and assuming a pf equal to one, the phase current is obtained.

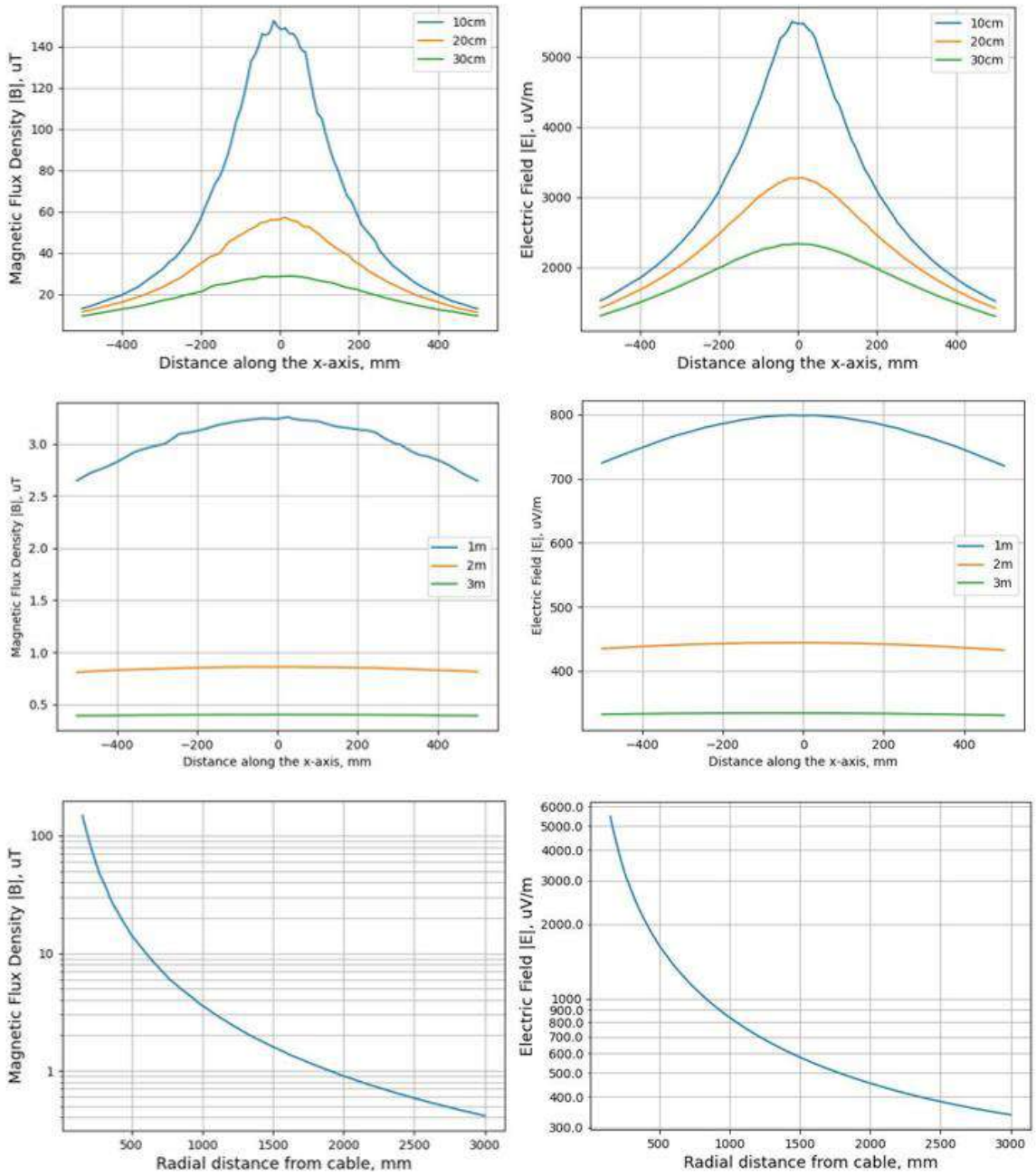

Figure 13. EMF modelling results from BiMEP submarine power cable at current carrying capacity at 10, 20, and 30 cm parallel to the cable surface (top); at 1, 2, and 3 m parallel to the cable surface (middle); and at a radial distance from the cable surface (bottom).

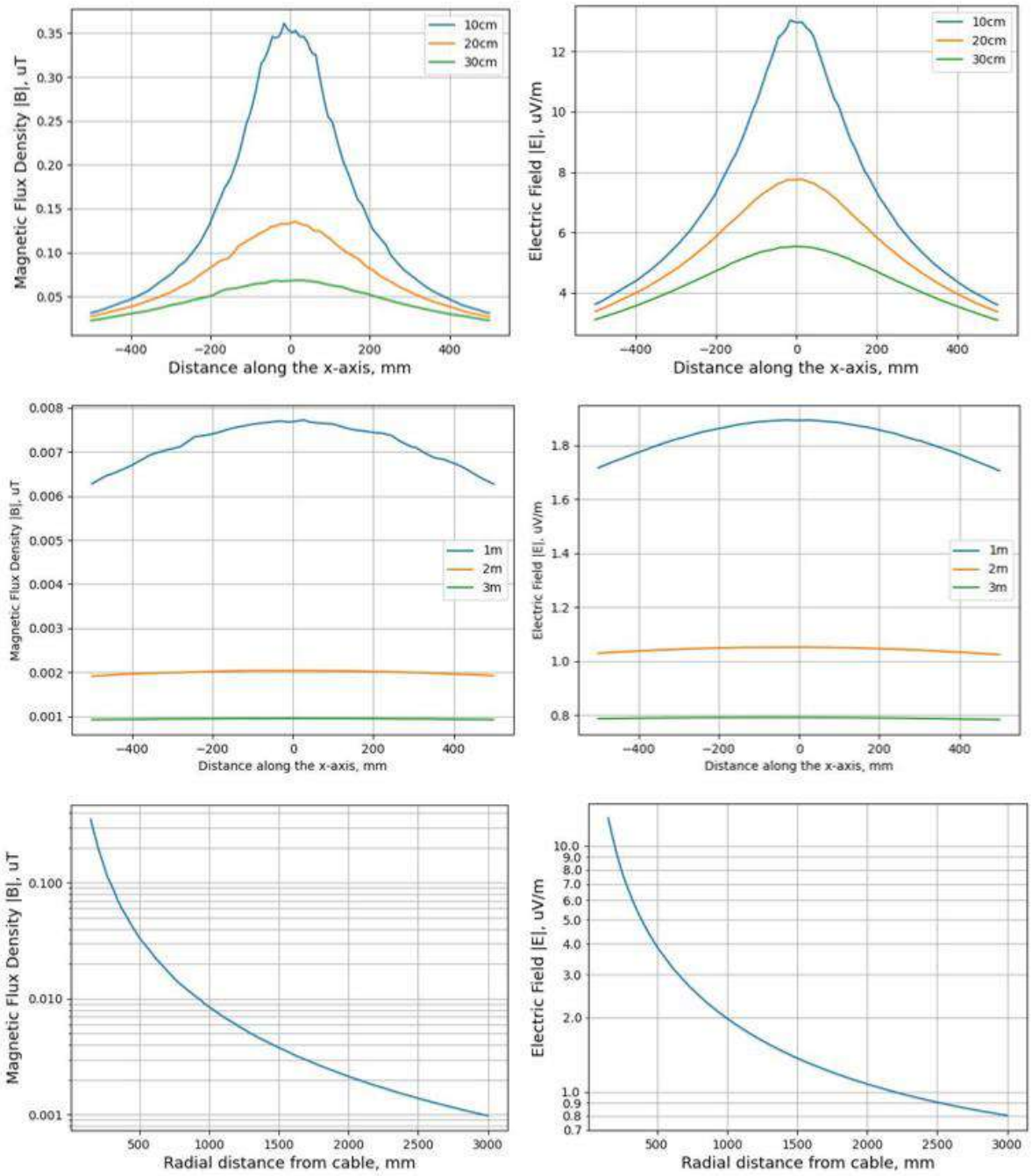

Figure 14. EMF modelling results from BiMEP submarine power cable per current unit at 10, 20, and 30 cm parallel to the cable surface (top); at 1, 2, and 3 m parallel to the cable surface (middle); and at a radial distance from the cable surface (bottom).

Table 8. Summary of the results at BiMEP test site.

	Total current	|B| at 10 cm	|B| at 3 m	|E| at 10 cm	|E| at 3 m
Cable ampacity	422 A	152.37	0.40 μT	5500.57 μV/m	334.33 μV/m
Unit current	1 A	0.36 μT	0.0009 μT	13.03 μV/m	0.79 μV/m
Device max. current	26.2 A	9.46 μT	0.02 μT	341.50 μV/m	20.76 μV/m

Table 9. Penguin II electrical specification

	P Device Rated Power	VLL Transmission Voltage	I Phase Current
Penguin II	600 kW	13.2 kV	26.2 A

The results obtained when the cable is energized with the unit of current can be used and scaled to obtain the levels of EMFs for the maximum current injected by the device. The following table summarizes the most relevant results in the case of rated cable current, unit of current and rated device current.

In Annex I, results at 20 cm, 30 cm, 1 m, and 2 m are also provided.

This same cable was studied in the previous WESE project returning results that are slightly lower than the ones presented above. In particular, at the cable ampacity (422 A) the maximum EMF obtained close to cable was 127 μT for the flux density and 4200 μV/m for the electric field (Chainho and Bald, 2021). This difference is due to the fact that the model used within SafeWAVE considers also a separation layer within the two armouring layers, in which is reasonable to consider some water infiltration that leads to higher EMF emissions.

5.3.3 SEM-REV Dynamic cable

The power cable under study is the dynamic umbilical cable connecting the energy device to a collection hub. As mentioned by Imperadore et al. (2023), at the time of the monitoring survey the 2 MW FLOATGEN wind turbine was the device connected to the cable and producing energy. The data collected

are used to validate the model by using the current monitored in the tool and comparing the output with the actual data monitored (see section Validation).

As mentioned in section SEM-REV Submarine Power Cable the cable is not buried, and natural burial has been disregarded since it could not be quantified. Moreover, it is to be expected that over time in the armour layers there might be some sea water infiltration.

Figure 15 shows the sketch of the cable under study, its model and the Finite Element Analysis performed on FEMM software.

For each simulation based on the cable geometry (see Figure 4) the cable model was created following the methodology described in section 5.2. Then, by applying the correct phase current characteristic of every simulation, and defining the mesh size, the FEMM solver was used to compute the EMF radiated as shown in the Figure 15.

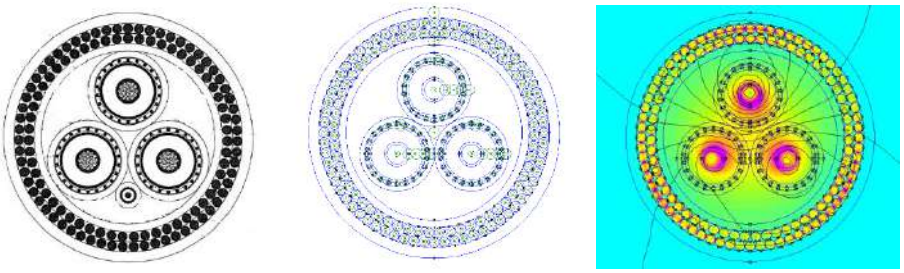

Figure 15. SEM-REV dynamic cable sketch (left); cable model in FEMM (centre); Finite Element Analysis in FEMM (right).

Below, the results from two simulations are reported, namely:

- Electric and magnetic field at cable ampacity (Figure 16).
- Electric and magnetic field per current unit (Figure 17).

Figure 16 presents the most relevant results because it allows to estimate the maximum values of EMFs to be expected when the cable is used at its maximum continuous current.

From

Table 4 the cable ampacity is known and equal to 246 A.

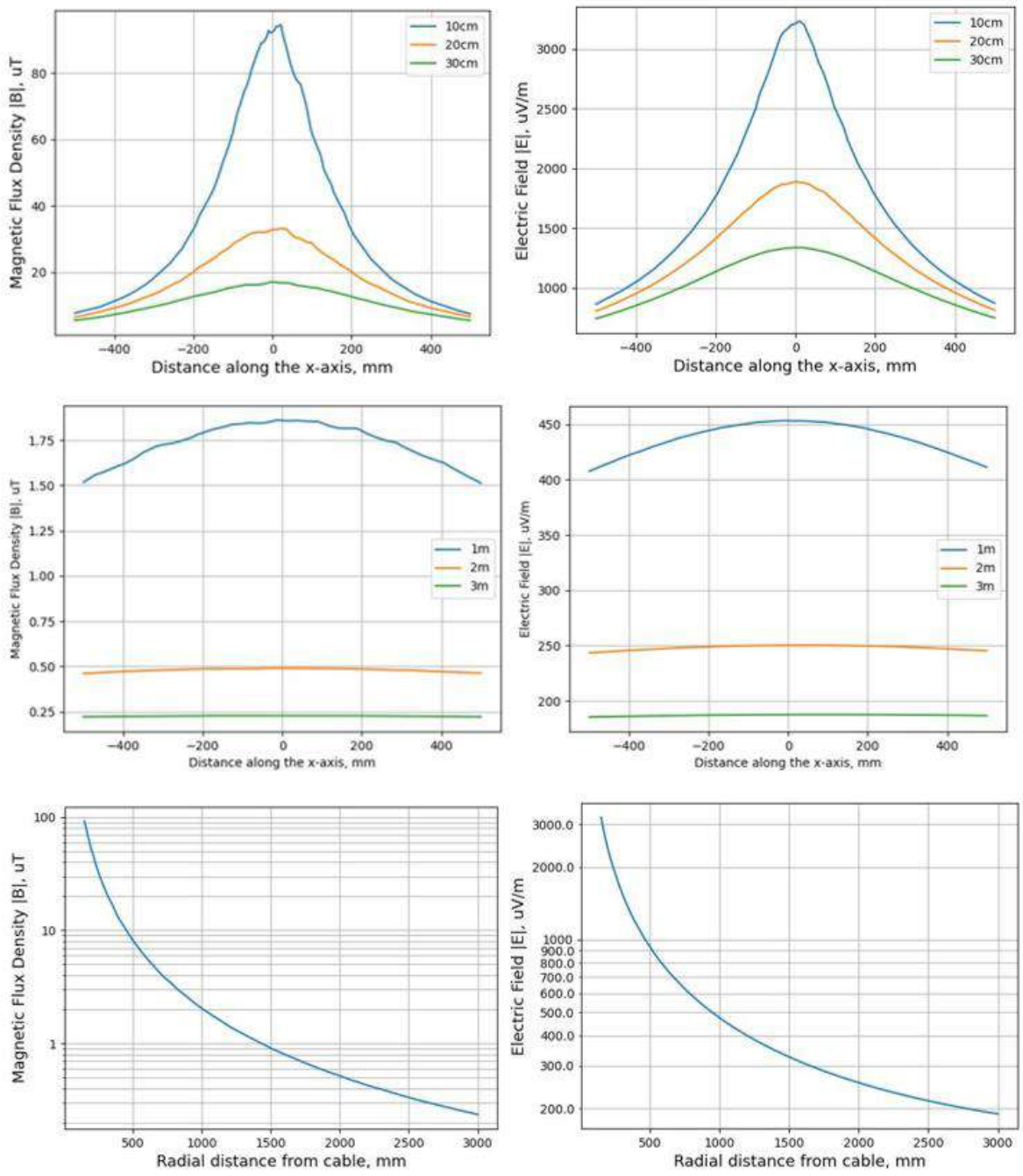

Figure 16. EMF modelling results from SEM-REV submarine dynamic power cable at cable current capacity at 10, 20, and 30 cm parallel to the cable surface (top); at 1, 2, and 3 m parallel to the cable surface (middle); and at a radial distance from the cable surface (bottom).

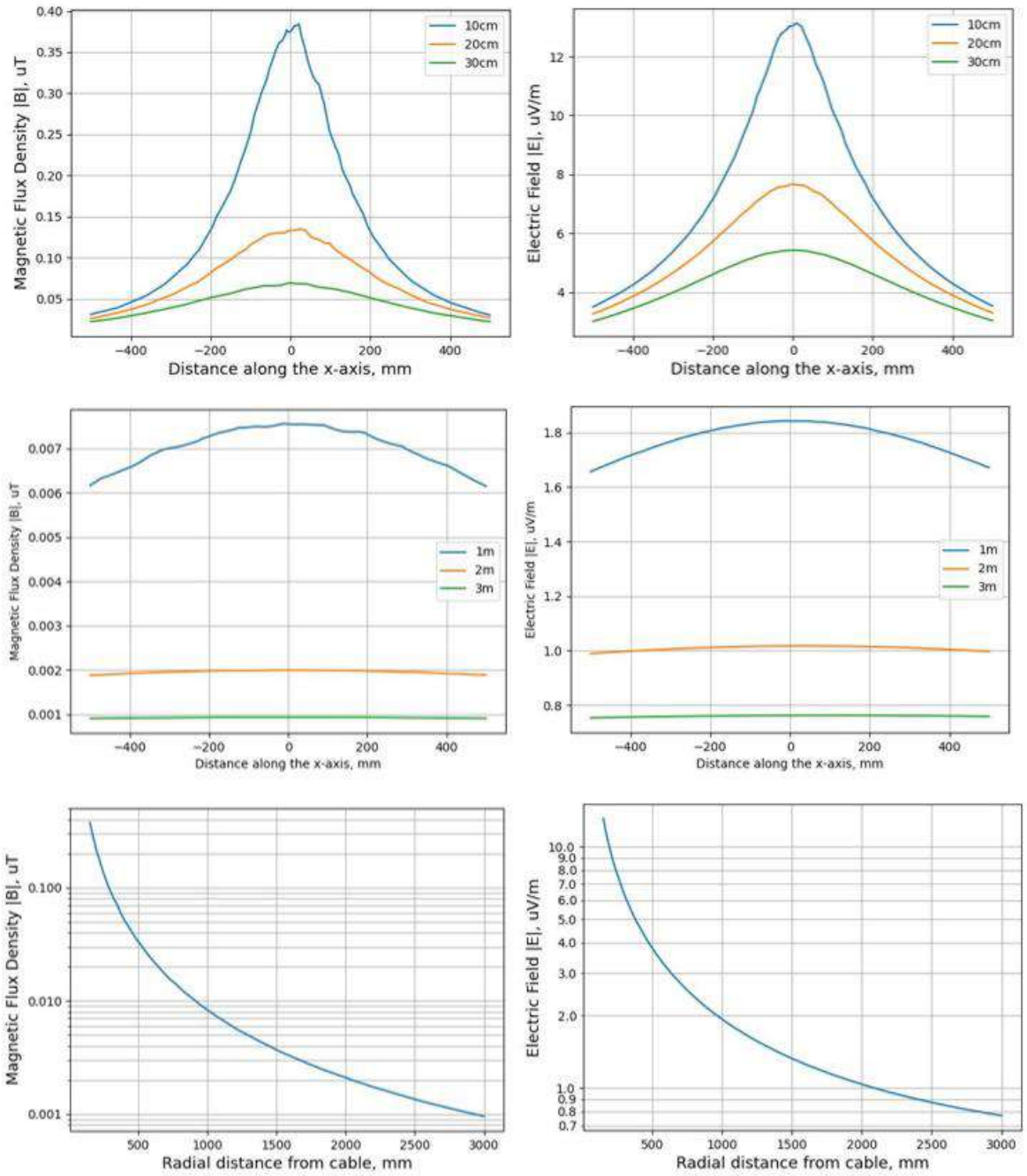

Figure 17. EMF modelling results from SEM-REV submarine dynamic power cable per current unit at 10, 20, and 30 cm parallel to the cable surface (top); at 1, 2, and 3 m parallel to the cable surface (middle); and at a radial distance from the cable surface (bottom).

At 10 cm from the cable the flux density |B| reaches 94.46 μT and at 3 m it reduces to 0.23 μT. The electric field follows the same trend, reaching its maximum of 3230.32 $\mu V/m$ at 10 cm from the cable and decaying to 187.65 $\mu V/m$ at 3 m (Table 10).

Table 10. Summary of the results at SEM-REV test site, dynamic cable.

	Total current	|B| at 10 cm	|B| at 3 m	|E| at 10 cm	|E| at 3 m
Cable ampacity	246 A	94.46 µT	0.23 µT	3230.32 µV/m	187.65 µV/m
Unit current	1 A	0.38 µT	0.0009 µT	13.13 µV/m	0.76 µV/m
Device max. current (FLOATGEN)	57.7 A	22.16 µT	0.05 µT	757.68 µV/m	44.01 µV/m
Device max. current (WAVEGEM)	4.33 A	1.69 µT	0.004 µT	56.72 µV/m	3.48 µV/m

Figure 17 shows results per current unit which can be used to estimate the magnitude of EMFs at any current level. Within the project scope it is relevant to estimate the EMF emissions when the device under study is at its rated power. As depicted in D2.2 (Imperadore et al., 2023), at the SEM-REV test site the device connected at the time of the survey was the FLOATGEN, a wind turbine with the electrical specifications reported in Table 11. Considering the following equation $P = \sqrt{3} \cdot V_{LL} \cdot I \cdot pf$ and assuming a pf equal to one, the phase current is obtained.

Table 11. FLOATGEN electrical specifications

	P Device Rated Power	VLL Transmission Voltage	I Phase Current
FLOATGEN	2 MW	20 kV	57.7 A

The results obtained when the cable is energized with the unit of current can be used and scaled to obtain the levels of EMFs for the maximum current injected by the device.

For this study case the FLOATGEN wind turbine is considered as power device because, as explained in Imperadore et al. (2023), at the time of the monitoring campaign it was the device energizing the cable. Nevertheless, the core of the project focuses on wave energy converter and at the test site it was previously installed (and later decommissioned) the 150 kW WAVEGEM wave energy converter from GEPS Techno. The results from the simulation at the WAVEGEM rated current are reported in the following table together with the results in case of the cable ampacity and per current unit. As expected, since the WEC device has a relevantly lower rated power than the wind turbine, maximum values are one order of magnitude lower.

In Annex I, results at 20 cm, 30 cm, 1 m, and 2 m are also provided.

5.3.4 SEM-REV Export cable

In this section the results from the modelling of the export cable at the SEM-REV test site are presented.

Figure 18 shows the sketch of the cable under study, its model and the Finite Element Analysis performed on the FEMM software.

As described in D2.2 (Imperadore et al., 2023), during the monitoring survey of the umbilical cable performed within this project the export cable was also depicted, and EMF data were collected at the time in which the FLOATGEN was operating. While the operating conditions are described in the Validation section, in this present one the simulations for the current at the cable rated power (Figure 19) and per unit current (Figure 20) are reported. The geometry of the cable is specified in Table 5.

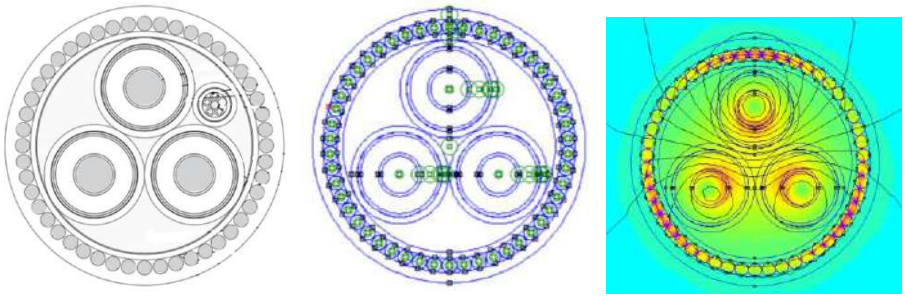

Figure 18. SEM-REV export cable sketch (left); cable model in FEMM (centre); Finite Element Analysis in FEMM (right).

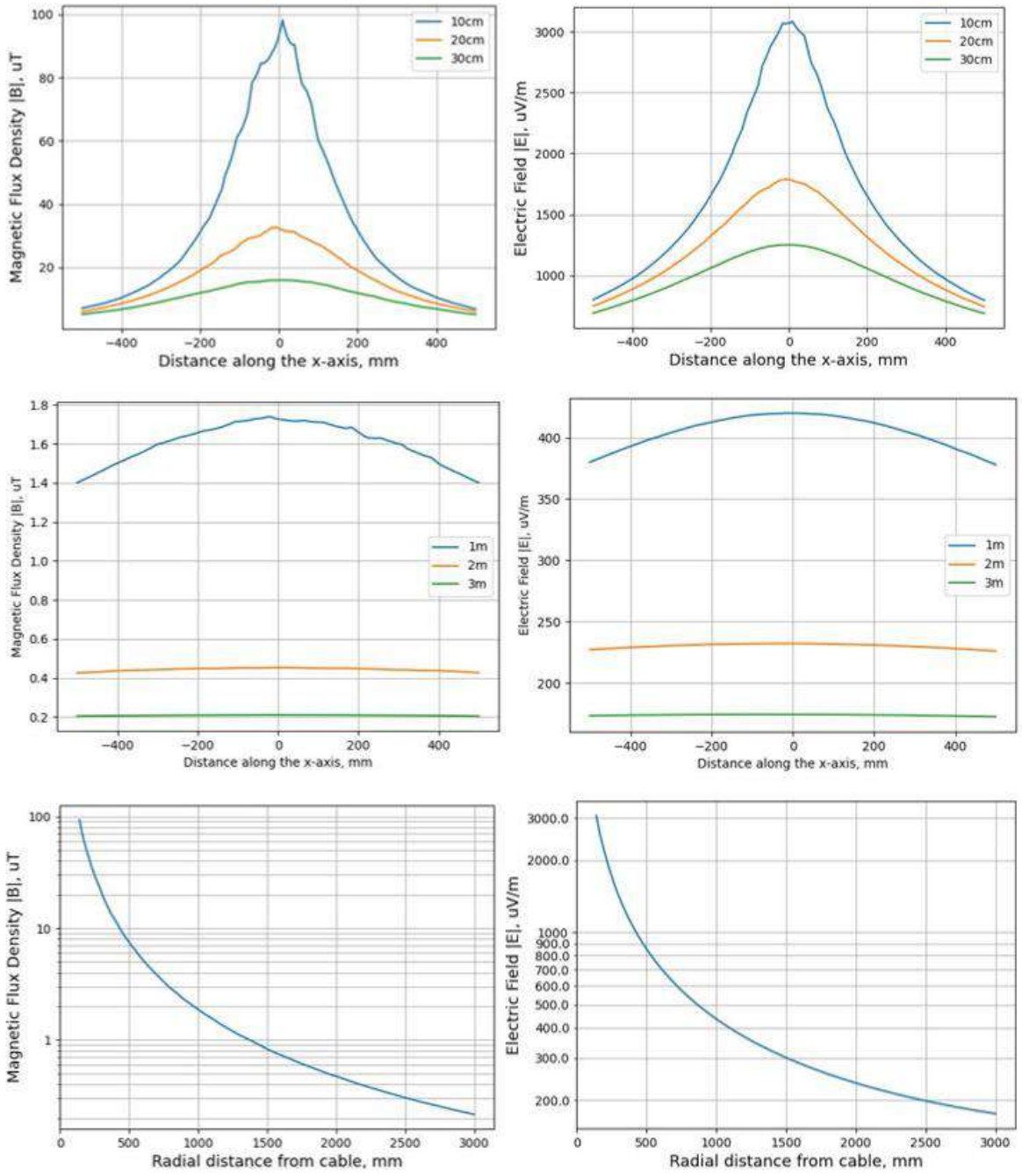

Figure 19. EMF modelling results from SEM-REV submarine export power cable at cable current capacity at 10, 20, and 30 cm parallel to the cable surface (top); at 1, 2, and 3 m parallel to the cable surface (middle); and at a radial distance from the cable surface (bottom).

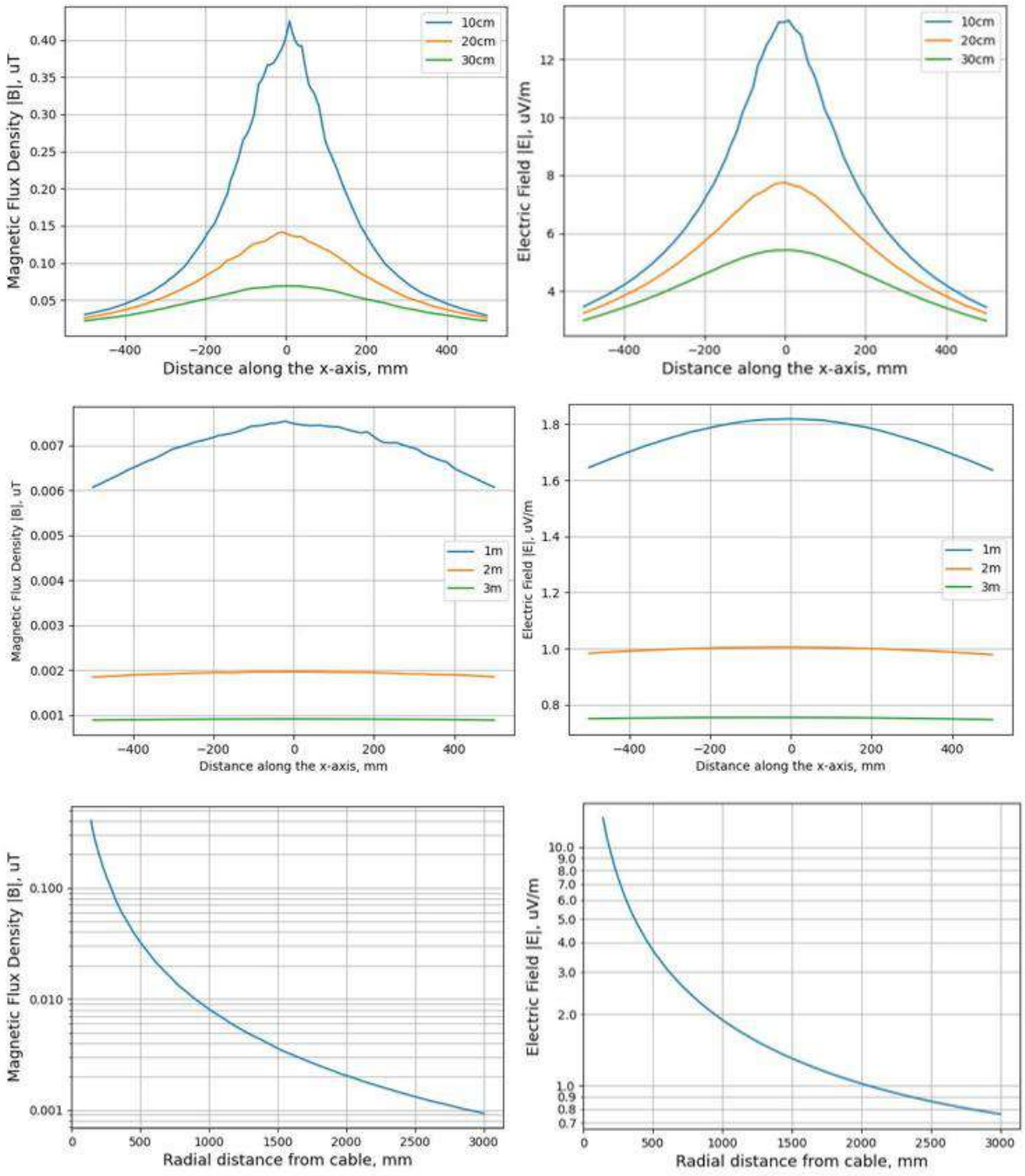

Figure 20. EMF modelling results from SEM-REV submarine export power cable per current unit at 10, 20, and 30 cm parallel to the cable surface (top); at 1, 2, and 3 m parallel to the cable surface (middle); and at a radial distance from the cable surface (bottom).

Differently to all the previous case studies, this cable is single-armoured and is buried at 1-1.5 m. On one side the emissions are expected to be lower because of the sand shielding the cable and on the other the armouring layer is thinner to contain the EMF emissions.

The cable is sized for 8 MVA and for a nominal voltage line-to-line of 20 kV, the resulting current is 230.9 A. Figure 19shows the results obtained at rated power for which at 10 cm from the seabed surface and parallel to the cable there is peak flux density of 98.22 μT, while at 3 m it reduces to 0.21 μT. For what it concerns the electrical field, at 10 cm distance the value is 3084.04 $\mu V/m$ and it reduces to 174.41 $\mu V/m$ at 3 m.

For both simulations the most relevant results are summarized in Table 12.

Table 12. Summary of the results at SEM-REV test site, export cable.

	Total current	**|B| at 10 cm**	**|B| at 3 m**	**|E| at 10 cm**	**|E| at 3 m**
Cable ampacity	230.9 A	98.22 μT	0.21 μT	3084.04 $\mu V/m$	174.41 $\mu V/m$
Unit current	1 A	0.42 μT	0.0009 μT	13.36 $\mu V/m$	0.75 $\mu V/m$

In Annex I, results at 20 cm, 30 cm, 1 m, and 2 m are also provided.

6. Validation

This section will present the results from the simulation performed by using the data collected during the monitoring campaign indicated in D2.2 (Imperadore et al., 2023).

At the time of writing Deliverable 2.2 (April 2023) the device at the BiMEP test site had already been decommissioned. The CPO's HiWave-5 was installed at the end of August 2023 and entered its first commissioning phase in October 2023. In the meantime, the device was removed from the site for maintenance at the end of November 2023 and was not redeployed within the SafeWAVE project timeline. Therefore no monitoring data are available to validate these two models created in the FEMM tool.

6.1 SEM-REV cable model validation

As depicted in D2.2 (Imperadore et al., 2023), the monitoring campaign returned average data of current and voltage that can be found in Table 13. Considering the equation for a three-phase system $P = \sqrt{3}.V_{LL}.I.pf$, where P is the power capacity, V_{LL} is the line-to-line voltage of the 3-phase transmission system, I is the phase current and pf is the power factor assumed to be equal to one, the power is calculated.

Table 13. FLOATGEN monitoring data at SEM-REV test site.

	Transmission voltage VLL (V)	Phase current I (A)	Power P (kW) calculated
FLOATGEN	11885.90	1.82	37.5

The set of results is shown in Figure 21 and it returns an amplitude of the magnetic field |B| of 0.70 μT at 10 cm from the cable, decaying to 1.7 nT at 3 m. Similarly, the electric field reaches a value of 23.90 $\mu V/m$ at 10 cm from the cable, decaying to 1.4 $\mu V/m$ at 3 m.

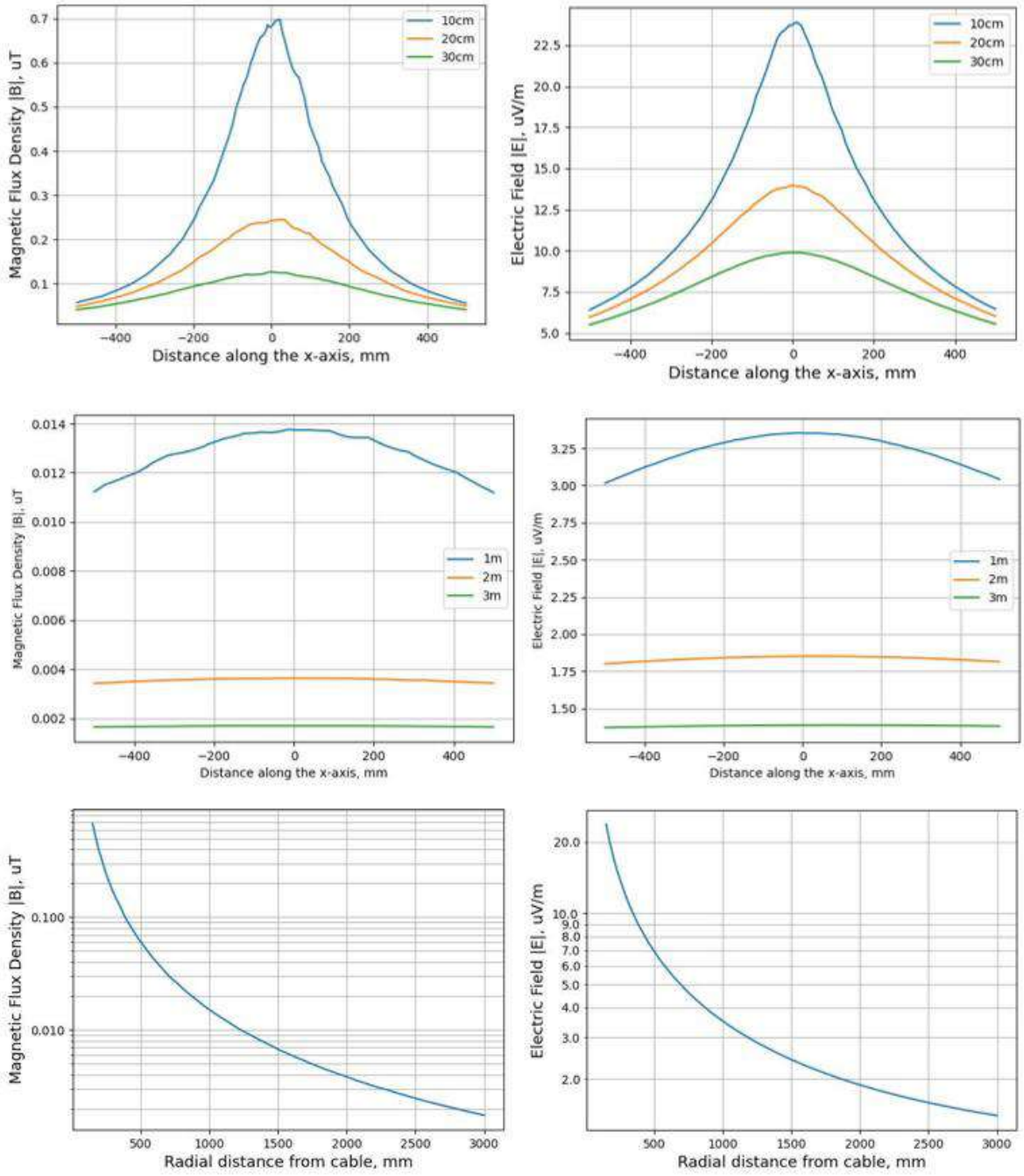

Figure 21. EMF modelling results from SEM-REV submarine power cable using the monitoring data at 10, 20, and 30 cm parallel to the cable surface (top); at 1, 2, and 3 m parallel to the cable surface (middle); and at a radial distance from the cable surface (bottom).

As described in D2.2 (Imperadore et al., 2023), the monitoring campaign was performed with a field sensor towed by an AUV that was travelling constantly at 3 m from the seabed. To validate the model, the available data from modelling and monitoring of EMF at 3 m from the seabed shall be compared. Nevertheless, the monitoring campaign returned only values of the magnetic field while the electric field is not known.

Among the different transects that the AUV travelled, the highest peak of magnetic field detected parallel to the cable surface and already deprived of the contribution of the geomagnetic field is 12.9 nT. It is to be noted that from the survey the current value of 1.82 is the average current with a deviation of 1.79, meaning that most probably the peak value of 12.9 nT corresponds to a higher value of current. This shall explain the difference between the peak value observed during the monitoring campaign and the peak value obtained with the modelling of the cable at 1.82 A of current.

This comparison does not allow to validate the model, nevertheless, both values are on the same order of magnitude (see Table 14) suggesting that the model is well representing the EMF emissions

Table 14. Monitoring and modelling magnitudes of flux density at 3 m distance from the cable at SEM-REV test site.

Average Current	|B| measured at 3 m	|B| modelled at 3 m
1.82 A	12.9 nT (max value)	1.7 nT

For the validation of the export cable, monitoring data from a campaign performed within the SPECIES project (https://www.france-energies-marines.org/en/projects/species/) are used.

By using a static measurement technique for a few tens of days it was possible to collect data of EMF emissions at 2 m from the collection hub and 10 m distance from the export cable.

At 5 m from the cable and a current of 55 A, which is the current close to the

rated power of the wind turbine (see Table 11), the peak magnetic density flux observed was 6 nT and the electric field of 16 $\mu V/m$.

By using the FEMM model of the export cable at 55 A, radial distributions of the magnetic field and the electric field are obtained (see Figure 22), in which at 5 m from the cable the flux density is equal to 0.03 μT and the electric field is equal to 38 $\mu V/m$.

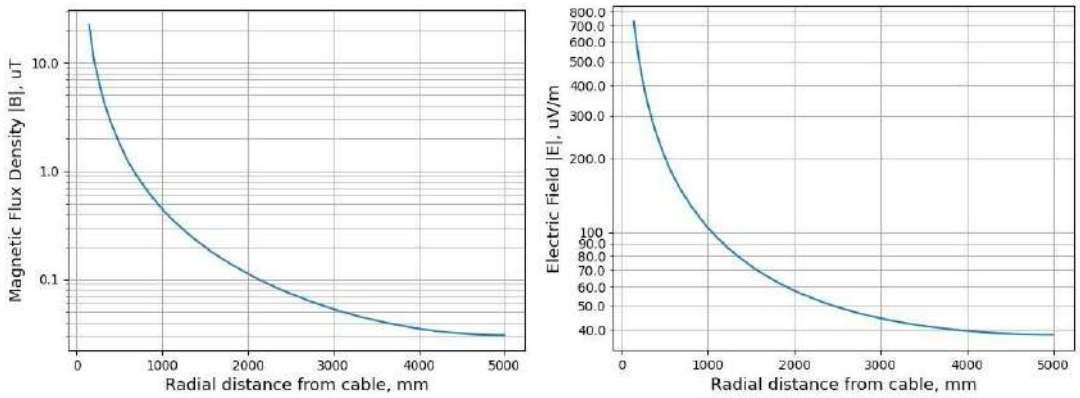

Figure 22. EMF modelling results of the export cable at SEM-REV using the monitoring data at a radial distance from the cable surface.

The comparison is not sufficient to validate the model, nevertheless in the monitoring campaign the field detected is probably representing a sum of different contributions. In fact, as shown in Figure 23, the sensor is placed close to the collection hub, the export cable and dynamic umbilical cable, meaning that the sensor is detecting an overall magnetic and electric field while the model is only simulating the EMF contribution of the export cable.

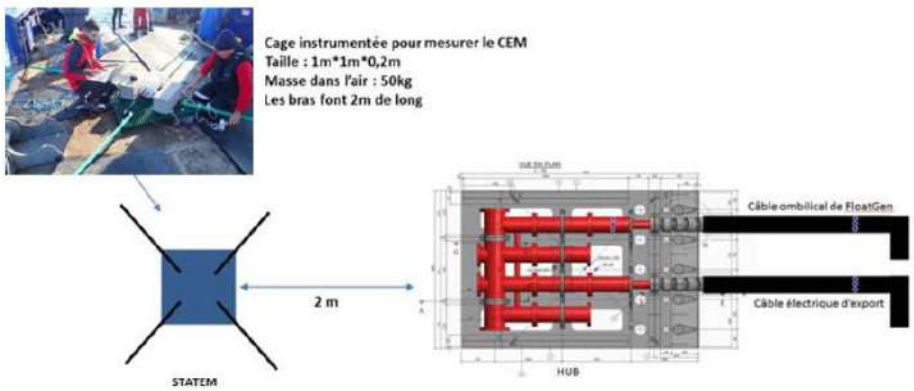

Figure 23. Diagram and picture of the STATEM© system. (Source: Reynaud et al., 2021).

7. Discussion and Conclusions

This Task aimed at estimating the levels of EMF generated by the power cables at three different test sites, namely the Aguçadoura, BiMEP and SEM-REV test sites. The goal was achieved by using a tool developed within the WESE project, which is an open-source tool capable of estimating the EMF distribution around a three-phase cable, based on Python and FEMM software. The tool was supposed to be validated using the monitoring data acquired under WP2 of WESE, but because the monitoring campaign could not be performed the tool's results were only compared to data found in literature.

SafeWAVE project emerged as a continuation of the WESE project and, despite not all the planned monitoring could be carried out, the data for the magnetic field from the SEM-REV test site are available and they were used to compare the results obtained with the power cable model. In section 6, the data collected during the campaign and the data obtained with the modelling show that the flux density is within the same order of magnitude but with slightly different values, in particular, the observed magnitude of $|\mathrm{B}|$ is higher than the one outputted from the model. The main cause to be attributed to this difference is related to the current that was flowing at the moment of the measurement. In fact, what was used for the simulation was an average value that certainly is not corresponding to the instantaneous value of current at the time in which the peak value of flux density was depicted.

The modelling tool allowed to obtain results relevant in the perspective of wider MRE farms that are likely to be developed in the next future. The results obtained for each power cable provide the maximum EMF to be expected in case of maximum exploitation of the cable, indicating when the cable is working at rated current, and the distance at which the EMF decays in case of the potential installation of new power cables. At present, the maximum magnetic and electric fields modelled considering the export cables capacity range between 174-5,501 $\mu\mathrm{V/m}$ (electric field) and 0.2-152 $\mu\mathrm{T}$ (magnetic field) at 10 cm and 3 m from the cable. The maximum fields obtained considering the devices capacity are much smaller, ranging between 18-342 $\mu\mathrm{V/m}$ (electric

field) and 0.02-10 μT (magnetic field) at 10 cm and 3 m from the cable.

There are numerous researchs reporting the potential detrimental effects of artificial EMF on marine animals, especially regarding fish or invertebrates. That is either on potential effects considering the organisms' ability of magneto- and/or electroreception to natural fields (e.g., Albert et al., 2020; Keller et al., 2021) or empirical trials observing the responses of organisms (at different life stages) to exposure to each or both fields (e.g., Fisher and Slater, 2010; Albert et al., 2020; Harsanyi et al., 2022). The literature shows that the probability and magnitude of detrimental effects of EMF depend greatly on the species, development stage, and environmental conditions, among other factors.

The magnetic fields modelled considering either the devices' maximum power production (maximum 10 μT at 10 cm from the export cable) or the export cables' maximum current capacity/ampacity (maximum 152 μT at 10 cm from the export cable) are quite below the values generally reported as having detrimental effects to marine animals (e.g., Fisher and Slater, 2010; Albert et al., 2020, 2022; Harsanyi et al., 2022). Nonetheless, some authors have reported behavioural (e.g., Hutchison et al., 2020) or physiological (e.g., Nishi et al., 2004) effects on animals exposed to magnetic fields in that range. As shown for some invertebrate species by Albert et al. (2020), while behavioural and/or physiological effects from artificial magnetic fields can be observed these may not necessarily mean changes to survival.

Compared to magnetic fields, fewer studies exist on the effects of artificial electric fields on marine animals. Nonetheless, some authors have shown behavioural and physiological effects, seemingly dependent both on the intensity (in $\mu V/m$) and the frequency (in Hz) of the fields. Considering that electric current in electric cables produces EMF at static frequencies (in the present case at 50 Hz) we will focus on the prior.

Elasmobranchs, the best studied electro-sensitive marine animals, can detect and use bioelectric potentials of very weak intensity (as low as 0.1 μV/m) and low frequency (<20 Hz) for orientation, foraging and prey capture, among others (e.g., Bedore and Kajiura, 2013; Newton et al., 2019). Bedore and Kajiura

(2013) determined that elasmobranchs produce a mean electric potential of 25 μV and that their preys (considering three families of invertebrates and eight families of fish) produce mean electric potentials of 17 μV (invertebrates) and 164 μV (teleost fish). Gill and Taylor (2001) showed individuals of the dogfish *Scyliorhinus canicula* being attracted to electric fields at 10 μV/m at 10 cm from the source. Examples of behavioural responses from other marine animal groups have been mentioned by Nyqvist et al. (2020), namely lampreys and eels observed to perceive laboratory electrical fields down to 100 μV/m and 67 μV/m, respectively, and the Guiana dolphin *Sotalia guianensis* being able to sense electric fields down to 460 μV/m. Direct physiological effects have also been reported. For example, Kalmijn (1966) showed the Thornback ray *Raja clavata* exhibited cardiac responses to uniform square-wave fields even at voltage gradients of 1 μV/m.

According to the above-mentioned, it might be possible that electric fields in the range of those modelled for a device at its maximum power production (18 μV/m at 3 m and 342 μV/m at 10 cm from the export cable) and for an export cable at its maximum current capacity (174 μV/m at 3 m and 5,501 μV/m at 10 cm from the export cable) overlap the fields precepted by predators, preys, or both, with potential effects at the individual level that might lead to consequences at the population level.

As highlighted by other authors (e.g., Hutchison et al., 2020, 2021), future research needs to involve not only research from the "stressor" perspective, i.e. artificial EMF measurement and modelling e.g. in relation to the cables characteristics, environment, and distance to cables, but also from the "receptor" perspective, i.e. considering the different effects at different life stages, for different species or focusing on particular species of interest, and the consequences at the population level. Further work should be dedicated to increase understanding on the effects caused in marine animals by EMF both at different intensity levels and at different frequency levels.

8. References

Albert, L., Deschamps, F., Jolivet, A., Olivier, F., Chauvaud, L., Chauvaud, S., 2020. A current synthesis on the effects of electric and magnetic fields emitted by submarine power cables on invertebrates. Marine Environmental Research 159, 104958.

Bedore, C.N., Kajiura, S.M., 2013. Bioelectric Fields of Marine Organisms: Voltage and Frequency Contributions to Detectability by Electroreceptive Predators. Physiological and Biochemical Zoology 86(3), p. 298-311.

Chainho, P., Bald, J., 2021. Deliverable 3.1 (EMF Modelling). Corporate deliverable of the WESE Project funded by the European Commission. Agreement number EASME/EMFF/2017/1.2.1.1/02/SI2.787640. 30 pp.

CMACS – Centre for Marine and Coastal Studies, 2003. A baseline assessment of electromagnetic fields generated by offshore windfarm cables. Birkenhead (UK), Centre for Marine and Coastal Studies, University of Liverpool: 71.

European Commission, 2020. Communication from the Commission to the European Parliament, the Council, the European Economic and Social Committee and the Committee of the Regions. An EU Strategy to harness the potential of offshore renewable energy for a climate neutral future. Brussels, 19.11.2020 COM(2020) 741 final.

Fisher, C., Slater, C., 2010. Electromagnetic Field Study – Effects of electromagnetic fields on marine species: a literature review. Report 0905-00-001 prepared on behalf of Oregon Wave Energy Trust. 23 pp.

Fleisch, D., 2008. A Student's Guide to Maxwell's Equations, Cambridge University Press, New York (USA). 134 pp.

Gill, A., Taylor, H., 2001. The Potential Effects of Electromagnetic Fields Generated by Cabling Between Offshore Wind Turbines upon Elasmobranch Fishes (Report No. 488). Report by Countryside Council for Wales. 60 pp.

Harsanyi, P., Scott, K., Easton, B.A.A., de la Cruz Ortiz, G., Chapman, E.C.N., Piper, A.J.R., Rochas, C.M.V., Lyndon, A.R., 2022 The Effects of Anthropogenic

Electromagnetic Fields (EMF) on the Early Development of Two Commercially Important Crustaceans, European Lobster, Homarus gammarus (L.) and Edible Crab, Cancer pagurus (L.). Journal of Marine Science and engineering 10, 564.

Hutchison, Z.L., Gill, A.B., Sigray, P., He, H., King, J.W., 2020. Anthropogenic electromagnetic fields (EMF) influence the behaviour of bottom-dwelling marine species. Scientific Reports 10, 4219.

Hutchison, Z.L., Gill, A.B., Sigray, P., He, H., King, J.W., 2021. A modelling evaluation of electromagnetic fields emitted by buried subsea power cables and encountered by marine animals: Considerations for marine renewable energy development. Renewable Energy 177, p. 72-81.

Imperadore, A., Amaral, L., Tanguy, F., Gregoire, Y., Vinagre, P.A., 2023. Deliverable 2.2 Monitoring of Electromagnetic fields. Corporate deliverable of the SafeWAVE Project co-funded by the European Maritime and Fisheries Fund (EMFF) program of the European Union, Call for Proposals EMFF-2019-1.2.1.1 - Environmental monitoring of ocean energy devices. 25 pp.

Kalmijn, A.J., 1966. Electro-perception in sharks and rays. Nature, Lond. 212, p. 1232-1233.

Keller, B.A., Putnam, N.F., Grubbs, R.D., Portnoy, D.S., Murphy, T.P., 2021. Map-like use of Earth's magnetic field in sharks. Current Biology, 31(13), p. 2881-2886.e3.

Meeker, D.C., "Finite Element Method Magnetics, Version 4.2 (21April 2019 Build)," [Online - https://www.femm.info/wiki/HomePage].

Newton, K.C., Gill, A.B., Kajiura, S.M., 2019. Electroreception in marine fishes: chondrichthyans. Journal of Fish Biology 95, p. 135-154.

Nishi, T., Kawamura, G., Matsumoto, K., 2004. Magnetic sense in the Japanese Eel, Anguilla japonica, as determined by conditioning and electrocardiography. The Journal of Experimental Biology 207, p. 2965-2970.

Nyqvist, D., Durif, C., Johnsen, M.G., De Jong, K., Forland, T.N., Sivle, L.D., 2020. Electric and magnetic senses in marine animals, and potential behavioral

effects of electromagnetic surveys. Marine Environmental Research 155, 104888.

Petkovska, L., Cvetkovski, G., 2005. Steady State Performance Evaluation of a Permanent Magnet Synchronous Motor Based on FEA.

Reynaud, M., Le Bourhis, E., Soulard, T., Perignon, Y., 2021. Rapport de suivi environnemental de l'éolienne flottante FLOATGEN, site d'essais SEM-REV. 87 pp.

Vinagre, P.A., Cruz, E., Chainho, P., Felis, I., Madrid, E., Soulard, T., Le Bourhis, E., Holm T., Le Berre, C., Bald, J., 2021. Deliverable 2.1 Development of Environmental monitoring plans. Corporate deliverable of the SafeWAVE Project co-funded by the European Maritime and Fisheries Fund (EMFF) program of the European Union, Call for Proposals EMFF-2019-1.2.1.1 - Environmental monitoring of ocean energy devices. 78 pp.

9. Annex I

Summary of the magnetic field modelling results for all test sites. (dyn: dynamic cable; exp: export cable)

Test site	Simulation	Current [A]	|B| 10 cm [µT]	|B| 20 cm [µT]	|B| 30 cm [µT]	|B| 1 m [µT]	|B| 2 m [µT]	|B| 3 m [µT]
CPO	Max cable current	274	98.85	33.45	16.86	1.83	0.48	0.22
CPO	Unit current	1	0.36	0.12	0.06	0.007	0.002	0.0008
CPO	Max device current	28.9	10.43	3.53	1.78	0.19	0.05	0.02
BiMEP	Max cable current	422	152.37	57.21	28.97	3.26	0.86	0.40
BiMEP	Unit current	1	0.36	0.14	0.07	0.008	0.002	0.0009
BiMEP	Max device current	26.2	9.46	3.55	1.80	0.20	0.05	0.02
SEM-REV dyn	Max cable current	246	94.46	33.15	17.12	1.86	0.49	0.23
SEM-REV dyn	Unit current	1	0.38	0.13	0.07	0.008	0.002	0.0009
SEM-REV dyn	Max device current (FLOATGEN)	57.7	22.16	7.78	4.02	0.44	0.11	0.05
SEM-REV dyn	Max device current (WAVEGEM)	4.33	1.69	0.59	0.29	0.03	0.009	0.004
SEM-REV exp	Max cable current	230.9	98.22	32.67	15.99	1.74	0.45	0.21
SEM-REV exp	Unit current	1	0.42	0.14	0.07	0.007	0.002	0.0009

Summary of the magnetic field modelling results for all test sites. (dyn: dynamic cable; exp: export cable)

est site	SImulation	Current [A]	|E| 10 cm [µV/m]	|E| 20 cm [µV/m]	|E| 30 cm [µV/m]	|E| 1 m [µV/m]	|E| 2 m [µV/m]	|E| 3 m [µV/m]
CPO	Max cable current	274	3232.10	1862.96	1314.27	435.50	236.20	174.84
CPO	Unit current	1	11.80	6.80	4.80	1.59	0.86	0.64
CPO	Max device current	28.9	340.90	196.50	138.62	45.93	24.91	18.44
BiMEP	Max cable current	422	5500.57	3279.33	2338.37	799.28	444.15	334.33
BiMEP	Unit current	1	13.03	7.77	5.54	1.89	1.05	0.79
BiMEP	Max device current	26.2	341.50	203.60	145.18	49.62	27.57	20.76
SEM-REV dyn	Max cable current	246	3230.32	1888.68	1336.79	453.40	250.32	187.65
SEM-REV dyn	Unit current	1	13.13	7.68	5.43	1.84	1.02	0.76
SEM-REV dyn	Max device current (FLOATGEN)	57.7	757.68	442.99	313.55	106.35	58.71	44.01
SEM-REV dyn	Max device current (WAVEGEM)	4.33	56.72	33.18	23.47	7.99	4.50	3.48
SEM-REV exp	Max cable current	230.9	3084.04	1788.82	1252.59	420.01	232.18	174.41
SEM-REV exp	Unit current	1	13.36	7.75	5.42	1.82	1.01	0.75